Available Online at www.jourcc.com

Journal homepage: www.JOURCC.com

Journal of Composites and Compounds

Corrosion behavior modeling and Montel Carlo simulation of a biomedical Ti–Zr–Nb–Ta alloy for dental applications

Tahereh Mahmoudi Alashti [a]*, ***Ketevan Mikeladze*** [b]*

[a] *Department of Medical Engineering, Islamic Azad University,South Tehran Branch, Tehran, Iran*

[b] *BAU International University, School of Medicine and Health Science, Batumi, Georgia*

ABSTRACT

The potentiodynamic polarization behavior of as-cast and accumulative roll-bonded (ARB) Ti–10Zr–5Nb–5Ta alloys was investigated in neutral Ringer solution at 37 °C to assess the influence of microstructural refinement on corrosion resistance and passivation. Using the Tafel equation, the potentiodynamic behavior of the as-cast and ARB-processed alloys was modeled to quantify electrochemical performance, with results indicating that ARB processing significantly modifies passive film characteristics. Model predictions were compared with experimental data, showing good agreement. The models were then coupled with Monte Carlo simulation to account for uncertainties in experimental data and fitting parameters, enabling probabilistic predictions of corrosion behavior. This integrated approach provides a robust evaluation of variability and reliability in electrochemical performance, offering a comprehensive assessment of the alloy's stability in physiological environments. The findings demonstrate that ARB processing can enhance corrosion resistance, supporting its potential for the development of durable titanium-based biomaterials for demanding biomedical and dental applications.

Peer review under responsibility of UGPH.

ARTICLE INFORMATION

Article History:
Received 01 April 2025
Received in revised form 10 June 2025
Accepted 27 June 2025

Keywords:
Potentiodynamic polarization behavior
As-cast process
Accumulative roll-bonded process
Modeling
Monte Carlo simulation
Dental application

1. Introduction

Owing to their high mechanical performance, remarkable resistance to corrosion, and favorable compatibility with biological tissues, titanium and its alloys are extensively utilized in implant fabrication [1, 2]. Among these, pure titanium and the ternary Ti–6Al–4V alloy are the materials most frequently utilized [3-6], largely because of their outstanding mechanical characteristics. However, studies have shown that ions released from Ti–6Al–4V, specifically vanadium and aluminum, can cause cytotoxicity and neurological issues, respectively [7, 8]. In addition, prolonged use of this alloy can result in inadequate load transmission to nearby bone, which in turn promotes bone resorption and eventual implant loosening [9-11].

For implant applications, a vanadium-free $\alpha + \beta$ alloy—most prominently Ti–6Al–7Nb—has also been employed [12-14]. The metal blend demonstrates outstanding strength, high resistance to corrosion, and good compatibility with biological tissues; however, its aluminum component has been associated with a higher likelihood of developing Alzheimer's disease [15].

The Ti–13Nb–13Zr alloy [7, 16-20] was developed as a near β-phase material, incorporating titanium, niobium, and zirconium—elements known for their biocompatibility [21, 22] and corrosion resistance. Additionally, the alloy exhibits a relatively low elastic modulus of approximately 80 GPa to 90 GPa, promoting improved osseointegration.

Since the addition of niobium and zirconium lowers the Young's modulus, researchers have developed new binary and ternary alloys with higher niobium content, including Ti–22Nb and Ti–22Nb–6Zr [23], as well as Ti–30Nb (around 100 GPa), Ti–30Nb–7.5Zr (about 70 GPa), and Ti–30Nb–15Zr (approximately 60 GPa) [24]. These alloys showed improved electrochemical stability under physiological conditions and heightened surface reactivity, both of which can support better osseointegration. In the last ten years, new quaternary alloys have been designed to fulfill the stringent demands for mechanical strength, corrosion resistance, and biocompatibility in implant applications. These alloys provide a unique combination of superior strength and fatigue durability while maintaining low density and elastic modulus, in addition to excellent wear resistance, biocompatibility, and corrosion resistance, all without exhibiting cytotoxic effects. Notable examples are the Ti–15Mo–5Zr–3Al [24, 25] and the Ti–5Al–2Nb–1Ta alloy [26] alloys, both of which have shown excellent mechanical and biological performance. The

* *Corresponding authors: Tahereh Mahmoudi Alashti & Ketevan Mikeladze, Emails: mt.mahmoudi1367@gmail.com, ketevan.mikeladze593@med.tsu.edu.ge*

https://doi.org/10.61882/jcc.7.2.5

Ti–15Zr–4Nb–4Ta alloy [27-29] is composed solely of non-toxic elements and exhibits outstanding mechanical strength, corrosion resistance, fatigue performance, and biocompatibility. Despite these advantages, its Young's modulus, at 97 GPa, still exceeds the typical range for bone, which lies between 6 and 20 GPa [30]. The β-phase Ti–29Nb–13Ta–4.6Zr alloy, composed exclusively of safe, non-toxic elements, features a Young's modulus of 60 GPa and maintains strong durability in Hank's physiological solution [31, 32]. The β-Ti alloys Ti–34Nb–9Zr–8Ta and Ti–13Mo–7Zr–3Fe, which exhibit a relatively low elastic modulus near 89 GPa, have been examined and shown to display a uniform microstructural arrangement. Two new alloys, Ti–29Nb–11Ta–5Zr and Ti–29Nb–6Ta–5Zr, were recently created using an electron-based design method and then manufactured [33]. Lowering the tantalum proportion from 11% to 6% led to a drop in the intrinsic elastic modulus, decreasing from 60 GPa to 43 GPa.

Another strategy is to apply combined thermo-mechanical processing to titanium alloys for biomedical use, aiming to achieve both enhanced strength and a reduced elastic modulus. Among these, Severe Plastic Deformation (SPD) techniques stand out as metal forming methods that introduce extremely large plastic strains into bulk materials, resulting in ultrafine-grained microstructures with exceptional mechanical properties [34, 35]. Within the family of SPD processes, Accumulative Roll Bonding (ARB) has emerged as a novel and effective method for bulk material fabrication. This technique involves repeated stacking and conventional roll bonding of materials [36]. ARB, when applied with an equivalent plastic strain exceeding 2, can produce ultrafine or nanocrystalline structures in multiphase bulk materials and even induce solid-state amorphization in multilayered systems [37]. The ARB process has successfully generated ultrafine and nanocrystalline microstructures in various metals, including titanium and its alloys [38, 39], interstitial-free steel [40, 41], and other materials [42, 43].

Raducanu and co-workers introduced a novel Ti–Zr–Nb–Ta multi-component alloy made exclusively from non-toxic elements and employed it to develop an advanced accumulative roll bonding (ARB) technique aimed at enhancing its microstructure and mechanical properties. The material exhibits a distinctive chemical structure within the realm of complex multi-element systems. Its design focuses on ensuring both local and systemic biocompatibility by including elements such as Ti, Zr, Nb, and Ta, which are known for their strong passivation and minimal ion release, making the alloy suitable for biomedical use. Furthermore, the composition is tailored to provide favorable mechanical performance, combining strength with a low elastic modulus through structural modifications. The ARB process has been applied to this alloy for the first time as a means to refine its microstructure, offering the added benefit of straightforward scalability compared to other severe plastic deformation methods. In their study, the mechanical properties and corrosion behavior of the ARB-processed Ti–10Zr–5Nb–5Ta (wt%) alloy were evaluated in a simulated body fluid and compared with those of the as-cast condition [44].

This study will evaluate and model the potentiodynamic polarization behavior of as-cast and ARB-processed Ti–10Zr–5Nb–5Ta alloys in neutral Ringer solution at 37 °C (as experimentally studied by Raducanu et al. [44]). The goal of this study is to evaluate key electrochemical parameters to better understand the influence of ARB processing on the alloy's corrosion resistance and passivation behavior. This evaluation is critical when considering the long-term stability and biocompatibility in a physiological environment for the implant and dental material uses of the alloys. Modelling the potentiodynamic behavior will clarify how parameters of microstructural refinement impact performance, and may ultimately aid the development of titanium-based biomaterials with greater durability and reliability for clinical use. Monte Carlo simulation will be included to consider the uncertainties related to the model parameters and experimental approaches. This gives rise to a probabilistic approach, which can provide a thorough reliability analysis of the corrosion predictions, supporting such understanding of the alloy's electrochemical performance. With respect to stability and suitability for demanding biomedical implant and dental applications where consistent corrosion resistance is important, the use of Monte Carlo simulation provides excellent support in this understanding.

2. Materials and methods

2.1. The Tafel equation

Julius Tafel (1863–1919) established a fundamental relationship in electrode kinetics in 1905, now known as the Tafel equation, often referred to as the "first law of electrode kinetics" [45]. This formula connects the overpotential (η) with the current density (j) in an electrochemical process, and can be written as:

$$\eta = a + blogj \tag{1}$$

where j is the current density in (A/cm^2), and a and b are constants determined experimentally. The parameters a and b are related to the exchange current density and charge transfer coefficient, respectively, and is determined using experimental data.

The overpotential, denoted as η, represents the deviation of the applied electrode potential, E, from the corrosion potential, E_{corr}, as defined below:

$$\eta = E - E_{corr} \tag{2}$$

Here, E is measured in volts (V).

This equation is derived as an approximation of the Butler-Volmer equation, which governs electrode kinetics by accounting for both anodic and cathodic processes:

$$j = j_0(e^{\frac{\alpha_a F\eta}{RT}} - e^{-\frac{\alpha_c F\eta}{RT}}) \tag{3}$$

In this equation, j stands for the net current density, J_0 is the exchange current density, α_a and α_c correspond to the anodic and cathodic charge transfer coefficients, F represents Faraday's constant, R is the universal gas constant, and T denotes the absolute temperature.

At sufficiently high anodic or cathodic overpotentials, one exponential term dominates and the other can be neglected. For large anodic overpotentials, the cathodic term is negligible, reducing the equation to:

$$j \approx j_0 e^{\frac{\alpha_a F\eta}{RT}} \tag{4}$$

Taking the logarithm of both sides produces the linear Tafel form, enabling extraction of kinetic parameters from experimental polarization data.

In the study of corrosion, the Tafel equation is commonly employed to obtain key metrics, like corrosion current density and corrosion potential, from polarization data, providing vital insight into the metal's corrosion performance under varying conditions. The Tafel slope reflects important mechanistic details such as charge transfer coefficients and electron transfer steps [45].

Within biomedical materials research, especially for titanium alloys, Tafel analysis is a key tool for evaluating passivation behavior and the robustness of protective oxide layers on alloy surfaces. Broad passive potential windows and minimal passive current densities, as revealed by Tafel curves, indicate superior

corrosion resistance and stable passive films, both of which are critical for implant longevity and biocompatibility [45].

2.2. Success probability: Probability of meeting design criteria

The parameters a, b, and E_{corr}, include uncertainties caused by measurement noise, variability among samples, and constraints in model fitting. To systematically assess the effect of these uncertainties on the model's predictions, Monte Carlo simulations are applied [46]. These parameters are drawn from probabilistic distributions defined by their confidence intervals. Integrating this stochastic approach with the equation outlined in Sec. 2.1 provides a robust method for evaluating how the probability of successful performance, where the system remains within its intended safe and operational limits, varies over the applied electrode potential.

3. Results and discussion

3.1. Modeling and validation for the potentiodynamic polarization behavior Ti–10Zr–5Nb–5Ta alloys in both their as-cast and ARB-processed forms

According to a study [44], the Ti–10Zr–5Nb–5Ta (wt%) alloy was fabricated via a cold crucible semi-levitation melting method, which ensured a homogeneous composition and prevented contamination during casting. The alloy underwent thermo-mechanical processing, including two stages of cold rolling with intermediate recrystallization at 850°C, resulting in precursor samples approximately 90 µm thick for the process of accumulative roll bonding (ARB). The ARB cycles involved repeated stacking, surface cleaning, and 50% thickness reduction rolling to achieve severe plastic deformation, performed three times in this study. Tensile and corrosion test specimens were machined from both as-cast and post-ARB alloy states, with tensile samples measuring 3 mm × 0.4 mm × 10 mm gauge length, and corrosion samples as 10 mm squares with 2 mm thickness. The corrosion behavior was assessed in Ringer's solution at 37 °C under aerated conditions. Cyclic potentiodynamic polarization experiments, conducted from −0.5 V to +2.0 V versus SCE, were used to determine corrosion and passivation potentials, current densities, and the stability of the passive film. Additionally, linear polarization measurements, performed within ±50 mV of the open circuit potential, provided values for polarization resistance, corrosion current density, corrosion rate, and ion release rates, calculated using standard equations. Now, the Tafel equation presented in Sec. 2.1 is employed to predict the potentiodynamic polarization behavior of both Ti–10Zr–5Nb–5Ta alloys, both in the as-cast state and after ARB processing, tested in neutral Ringer's solution at 37 °C. For this purpose, the experimental dataset from Raducanu et al. [44] was divided into a training subset and a testing subset. The training subset was utilized to estimate the unknown parameters in Eq. (1), while the testing subset served to evaluate the predictive accuracy of the model. The training dataset is used to estimate the unknown parameters in Eq. (1), and the relationship between current density and applied electrode potential for both for Ti–10Zr–5Nb–5Ta alloys in either the as-cast or ARB-processed state is presented as follows:

$$j = 10^{0.88(-5.39+E)} \quad \textit{for Ti–10Zr–5Nb–5Ta alloys in as-cast processed form} \tag{5}$$

$$j = 10^{0.84(-6.67+E)} \quad \textit{for Ti–10Zr–5Nb–5Ta alloys in ARB-processed form} \tag{6}$$

Since the Tafel equation inherently expresses the relationship between overpotential (η) and the logarithm of the current density ($logj$), the comparison between model predictions and experimental data was performed in the logarithmic domain. The predicted $logj$ values obtained from the model are plotted against the corresponding experimental $logj$. Fig. 1 illustrates the comparison between the predicted and measured current density of Ti–10Zr–5Nb–5Ta alloys in either the as-cast or ARB-processed state. The findings demonstrate a good agreement between the model's predictions and experimental data, confirming that the developed model reliably estimates the current density for the as-cast and ARB-modified Ti–10Zr–5Nb–5Ta alloys, with overall coefficients of variation of 3.75% and 2.14%, respectively, based on the test dataset [44]. In Fig. 2 The corrosion behavior of as-cast and ARB-modified Ti–10Zr–5Nb–5Ta alloys was evaluated in neutral Ringer's solution at 37 °C, revealing significant improvements in corrosion resistance following ARB processing. The ARB alloy exhibited substantially lower corrosion current densities across the entire potential range, starting at approximately $10^{-5.95}$ A/cm² compared to $10^{-5.11}$ A/cm² for the as-cast alloy, and maintaining this advantage even at higher potentials ($10^{-3.93}$ A/cm² vs. $10^{-2.99}$ A/cm²). This reduction in current density indicates a slower corrosion rate and suggests the formation of a more stable and protective passive oxide film on the ARB alloy surface.

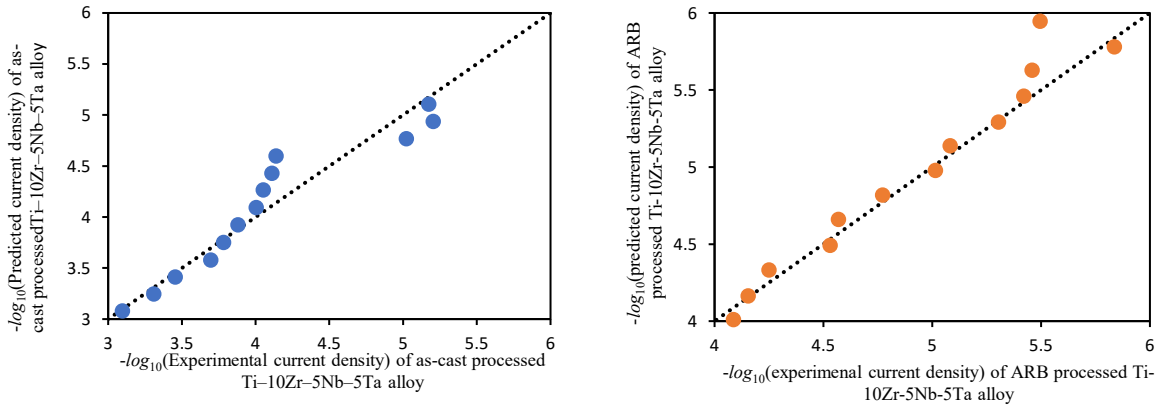

(a) (b)

Fig. 1. Comparison of the logarithm of predicted and measured [44] current density of (a) the as-cast and (b) the ARB processed Ti–10Zr–5Nb–5Ta alloys [44].

In contrast, the as-cast alloy demonstrated higher current densities, implying less effective passivation or a more rapid breakdown of the passive layer. Although exact corrosion potentials were not explicitly determined, the ARB alloy is inferred to possess a more noble corrosion potential, consistent with its enhanced corrosion resistance. Such enhancements result from microstructural refinement and the elimination of defects caused ARB process, which facilitate the formation of a uniform, stable passive layer and improve the alloy's performance in physiological environments.

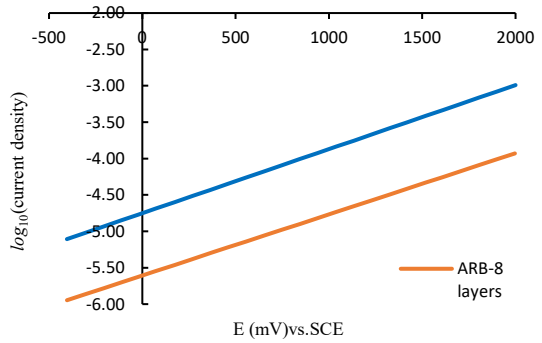

Fig. 2. Potentiodynamic curves for as-cast and ARB-modified Ti–10Zr–5Nb–5Ta alloys.

3.2. Success probability: Probability of meeting design criteria for the potentiodynamic polarization behavior of Ti–10Zr–5Nb–5Ta alloys in both their as-cast and ARB-processed forms

This work utilizes the experimental results reported by Raducanu et al. [44] to formulate the limit state functions (LSFs). Drawing on the potentiodynamic behavior data of the as-cast and ARB-modified Ti–10Zr–5Nb–5Ta alloys, as presented in the previous section, the LSFs are defined as follows:

$$\log i < -5 \tag{7}$$

The parameters a, b, and E_{corr}, in Eq. (1), are considered using normal probability distributions. Their specific attributes are listed in Table 1 for the as-cast and ARB-modified Ti–10Zr–5Nb–5Ta alloys. To assess the probability of success, 100,000 random values are produced for each parameter within their defined limits. These values are then employed to determine the chance that the logarithm of current density remain inside the designated functional safety zone, based on the established model.

Table 1
Parameter ranges applied in the Monte Carlo simulation, adapted from Raducanu et al. [44].

Parameters	Process	Mean (μ)	Std. Dev. (σ)
a	as-cast	5.84	0.2
b	as-cast	1.13	0.05
E_{corr}	as-cast	-0.45	0.01
a	ARB	7.12	0.2
b	ARB	1.19	0.05
E_{corr}	ARB	-0.45	0.01

Fig. 3 shows the computed success probabilities of logarithm of current density in terms of applied voltage. The orange and blue circular markers, respectively, represent data obtained from Monte Carlo simulations of the current density of as-cast and ARB-modified Ti–10Zr–5Nb–5Ta alloys, while the overlaid polynomial regression curves are fitted to these data points. In the regression equations, y denotes the success probability and x represents applied voltage. It is obtained that the success probability of the as-cast and ARB-modified Ti–10Zr–5Nb–5Ta alloys is lower than the success probability for ARB processed Ti–10Zr–5Nb–5Ta alloy.

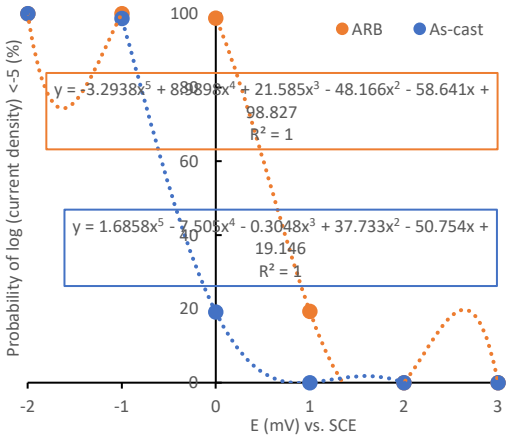

Fig. 3. The success probability of *log*(current density) in terms of applied voltage for Ti–10Zr–5Nb–5Ta alloys in both their as-cast and ARB-processed forms.

4. Conclusion

Considering the experimental database in Ref. [44], the corrosion behavior of as-cast and accumulative roll-bonded (ARB) Ti–10Zr–5Nb–5Ta alloys in neutral Ringer's solution at 37 °C was modeled. The Tafel-based model reliably predicted current densities, exhibiting low coefficients of variation of 3.75% for the as-cast alloy and 2.14% for the ARB-processed alloy, demonstrating strong agreement with experimental data. The ARB-processed alloy showed significantly lower corrosion current densities across the potential range, indicating slower corrosion rates and the formation of a more stable, protective passive oxide film compared to the as-cast alloy.

These improvements are attributed to microstructural refinement and defect reduction resulting from ARB processing, which promote a uniform and durable passive layer. Monte Carlo simulations further enhanced the analysis by providing a probabilistic evaluation that accounts for uncertainties in both measurements and model parameters. Overall, these findings confirm that ARB processing improves corrosion resistance and enables accurate performance predictions, supporting its potential for producing durable titanium-based biomaterials for demanding biomedical and dental applications.

Author contributions

Tahereh Mahmoudi Alashti: Writing – original draft, Writing – review & editing; **Ketevan Mikeladze:** Writing – original draft, Writing – review & editing, Conceptualization**.**

Funding

No funding was received for this study.

Conflict of interest

The authors declare no conflict of interest.

Data availability

No data is available

REFERENCES

[1] M. Niinomi, Mechanical biocompatibilities of titanium alloys for biomedical applications, Journal of the mechanical behavior of biomedical materials 1(1) (2008) 30–42.
[2] L. Murr, S. Quinones, S. Gaytan, M. Lopez, A. Rodela, E. Martinez, D. Hernandez, E. Martinez, F. Medina, R. Wicker, Microstructure and mechanical behavior of Ti–6Al–4V produced by rapid-layer manufacturing, for biomedical applications, Journal of the mechanical behavior of biomedical materials 2(1) (2009) 20–32.
[3] M. Khan, R. Williams, D. Williams, In-vitro corrosion and wear of titanium alloys in the biological environment, Biomaterials 17(22) (1996) 2117–2126.
[4] S. Tamilselvi, R. Murugaraj, N. Rajendran, Electrochemical impedance spectroscopic studies of titanium and its alloys in saline medium, Materials and Corrosion 58(2) (2007) 113–120.
[5] A. Guitar, G. Vigna, M. Luppo, Microstructure and tensile properties after thermohydrogen processing of Ti–6Al–4V, Journal of the Mechanical Behavior of Biomedical Materials 2(2) (2009) 156–163.
[6] C. Ramos-Saenz, P. Sundaram, N. Diffoot-Carlo, Tribological properties of Ti-based alloys in a simulated bone–implant interface with Ringer's solution at fretting contacts, Journal of the mechanical behavior of biomedical materials 3(8) (2010) 549–558.
[7] M. Geetha, A. K. Singh, R. Asokamani, A. K. Gogia, Ti based biomaterials, the ultimate choice for orthopaedic implants–A review, Progress in materials science 54(3) (2009) 397–425.
[8] G. Van der Voet, E. Marani, S. Tio, F. De Wolff, Aluminium neurotoxicity, Progress in histochemistry and cytochemistry 23(1-4) (1991) 235–242.
[9] N. Abavi Torghabeh, R. Pouriamanesh, A review on Ti-based metal matrix composite coatings, Journal of Composites and Compounds 4(13) (2022) 209–219.
[10] M. Reisi Nafchi, R. Ebrahimi-kahrizsangi, Synthesis of Zn-Co-TiO2 nanocomposite coatings by electrodeposition with photocatalytic and antifungal activities, Journal of Composites and Compounds 3(9) (2021) 213–217.
[11] V. P. S. Sidhu, R. Borges, M. Yusuf, S. Mahmoudi, S. F. Ghorbani, M. Hosseinikia, P. Salahshour, F. Sadeghi, M. Arefian, A comprehensive review of bioactive glass: synthesis, ion substitution, application, challenges, and future perspectives, Journal of Composites and Compounds 3(9) (2021) 247–261.
[12] M. F. López, L. Soriano, F. J. Palomares, M. Sánchez-Agudo, G. Fuentes, A. Gutiérrez, J. A. Jiménez, Soft x-ray absorption spectroscopy study of oxide layers on titanium alloys, Surface and Interface Analysis: An International Journal devoted to the development and application of techniques for the analysis of surfaces, interfaces and thin films 33(7) (2002) 570–576.
[13] M. F. López, J. A. Jiménez, A. Gutierrez, Corrosion study of surface-modified vanadium-free titanium alloys, Electrochimica Acta 48(10) (2003) 1395–1401.
[14] C. Morant, M. F. López, A. Gutiérrez, J. A. Jiménez, AFM and SEM characterization of non-toxic vanadium-free Ti alloys used as biomaterials, Applied Surface Science 220(1-4) (2003) 79–87.
[15] S. Rao, Y. Okazaki, T. Tateishi, T. Ushida, Y. Ito, Cytocompatibility of new Ti alloy without Al and V by evaluating the relative growth ratios of fibroblasts L929 and osteoblasts MC3T3-E1 cells, Materials Science and Engineering: C 4(4) (1997) 311–314.
[16] S. Yu, J. Scully, Corrosion and passivity of Ti-13% Nb-13% Zr in comparison to other biomedical implant alloys, Corrosion 53(12) (1997) 965–976.
[17] S. L. de Assis, S. Wolynec, I. Costa, Corrosion characterization of titanium alloys by electrochemical techniques, Electrochimica Acta 51(8-9) (2006) 1815–1819.
[18] S. L. d. Assis, I. Costa, Electrochemical evaluation of Ti-13Nb-13Zr, Ti-6Al-4V and Ti-6Al-7Nb alloys for biomedical application by long-term immersion tests, Materials and Corrosion 58(5) (2007) 329–333.
[19] S. L. d. Assis, S. Wolynec, I. Costa, The electrochemical behaviour of Ti-13Nb-13Zr alloy in various solutions, Materials and Corrosion 59(9) (2008) 739–743.
[20] A. Robin, O. Carvalho, S. Schneider, S. Schneider, Corrosion behavior of Ti-xNb-13Zr alloys in Ringer's solution, Materials and corrosion 59(12) (2008) 929–933.
[21] P. Thomsen, C. Larsson, L. Ericson, L. Sennerby, J. Lausmaa, B. Kasemo, Structure of the interface between rabbit cortical bone and implants of gold, zirconium and titanium, Journal of Materials Science: Materials in Medicine 8(11) (1997) 653–665.
[22] E. Eisenbarth, D. Velten, M. Müller, R. Thull, J. Breme, Biocompatibility of β-stabilizing elements of titanium alloys, Biomaterials 25(26) (2004) 5705–5713.
[23] B. Wang, Y. Zheng, L. Zhao, Electrochemical corrosion behavior of biomedical Ti–22Nb and Ti–22Nb–6Zr alloys in saline medium, Materials and Corrosion 60(10) (2009) 788–794.
[24] D. Q. Martins, W. R. Osório, M. E. Souza, R. Caram, A. Garcia, Effects of Zr content on microstructure and corrosion resistance of Ti–30Nb–Zr casting alloys for biomedical applications, Electrochimica Acta 53(6) (2008) 2809–2817.
[25] W.-S. Lee, C.-F. Lin, T.-H. Chen, H.-H. Hwang, Effects of strain rate and temperature on mechanical behaviour of Ti–15Mo–5Zr–3Al alloy, Journal of the mechanical behavior of biomedical materials 1(4) (2008) 336–344.
[26] S. Tamilselvi, N. Rajendran, In vitro corrosion behaviour of Ti-5Al-2Nb-1Ta alloy in Hanks solution, Materials and Corrosion 58(4) (2007) 285–289.
[27] Y. Okazaki, A new Ti–15Zr–4Nb–4Ta alloy for medical applications, Current Opinion in Solid State and Materials Science 5(1) (2001) 45–53.
[28] Y. Okazaki, E. Nishimura, H. Nakada, K. Kobayashi, Surface analysis of Ti–15Zr–4Nb–4Ta alloy after implantation in rat tibia, Biomaterials 22(6) (2001) 599–607.
[29] Y. Okazaki, S. Rao, Y. Ito, T. Tateishi, Corrosion resistance, mechanical properties, corrosion fatigue strength and cytocompatibility of new Ti alloys without Al and V, Biomaterials 19(13) (1998) 1197–1215.
[30] P. Zysset, X. Guo, C. Hoffler, K. Moore, S. Goldstein, Mechanical properties of human trabecular bone lamellae quantified by nanoindentation, Technology and Health Care 6(5-6) (1998) 429–432.
[31] M. Karthega, V. Raman, N. Rajendran, Influence of potential on the electrochemical behaviour of β titanium alloys in Hank's solution, Acta biomaterialia 3(6) (2007) 1019–1023.
[32] Y. Tanaka, M. Nakai, T. Akahori, M. Niinomi, Y. Tsutsumi, H. Doi, T. Hanawa, Characterization of air-formed surface oxide film on Ti–29Nb–13Ta–4.6 Zr alloy surface using XPS and AES, corrosion Science 50(8) (2008) 2111–2116.
[33] P. Laheurte, F. Prima, A. Eberhardt, T. Gloriant, M. Wary, E. Patoor, Mechanical properties of low modulus β titanium alloys designed from the electronic approach, Journal of the mechanical behavior of biomedical materials 3(8) (2010) 565–573.
[34] A. Azushima, R. Kopp, A. Korhonen, D.-Y. Yang, F. Micari, G. Lahoti, P. Groche, J. Yanagimoto, N. Tsuji, A. Rosochowski, Severe plastic deformation (SPD) processes for metals, CIRP annals 57(2) (2008) 716–735.
[35] I. J. Beyerlein, L. S. Tóth, Texture evolution in equal-channel angular extrusion, Progress in Materials Science 54(4) (2009) 427–510.
[36] Y. Saito, H. Utsunomiya, N. Tsuji, T. Sakai, Novel ultra-high straining process for bulk materials—development of the accumulative roll-bonding (ARB) process, Acta materialia 47(2) (1999) 579–583.
[37] R. Hebert, J. Perepezko, Deformation-induced synthesis and structural transformations of metallic multilayers, Scripta materialia 50(6) (2004) 807–812.
[38] G. Dinda, H. Rösner, G. Wilde, Synthesis of bulk nanostructured Ni, Ti and Zr by repeated cold-rolling, Scripta materialia 52(7) (2005) 577–582.
[39] R. Zhang, V. L. Acoff, Processing sheet materials by accumulative roll bonding and reaction annealing from Ti/Al/Nb elemental foils, Materials Science and Engineering: A 463(1-2) (2007) 67–73.
[40] N. Tsuji, R. Ueji, Y. Minamino, Nanoscale crystallographic analysis of ultrafine grained IF steel fabricated by ARB process, Scripta Materialia 47(2) (2002) 69–76.
[41] N. Kamikawa, T. Sakai, N. Tsuji, Effect of redundant shear strain on microstructure and texture evolution during accumulative roll-bonding in ultralow carbon IF steel, Acta Materialia 55(17) (2007) 5873–5888.
[42] M. Shaarbaf, M. R. Toroghinejad, Nano-grained copper strip produced by accumulative roll bonding process, Materials Science and Engineering: A 473(1-2) (2008) 28–33.
[43] P. Hsieh, J. Huang, Y. Hung, S. Chou, J. Jang, Characterization on nanocrystallization and amorphization evolution in Zr–X alloys during ARB process, Materials chemistry and physics 88(2-3) (2004) 364–376.
[44] D. Raducanu, E. Vasilescu, V. Cojocaru, I. Cinca, P. Drob, C. Vasilescu, S. Drob, Mechanical and corrosion resistance of a new nanostructured Ti–Zr–Ta–Nb alloy, Journal of the mechanical behavior of biomedical materials 4(7) (2011) 1421–1430.
[45] J. Tafel, Über die Polarisation bei kathodischer Wasserstoffentwicklung, Zeitschrift für physikalische Chemie 50(1) (1905) 641–712.
[46] M. Khamehchi, A. Chkhenkeli, Influence of Ionic Size on the concentration of Ag+ and Zn2+ in Simulated Body Fluid: Modeling and Monte Carlo Simulation with Dental Applications, Journal of Composites and Compounds 6(21) (2024).